

DIRECTIONAL VARIATIONS OF THE NON-GAUSSIANITY PARAMETER f_{NL}

ØYSTEIN RUDJORD^{1,2,3}, FRODE K. HANSEN^{2,3}, XIAOHONG LAN⁴
MICHELE LIGUORI⁵ DOMENICO MARINUCCI⁴ SABINO MATARRESE⁶

Draft version November 11, 2018

ABSTRACT

We investigate local variations of the primordial non-Gaussianity parameter f_{NL} in the WMAP data, looking for possible influence of foreground contamination in the full-sky estimate of f_{NL} . We first improve the needlet bispectrum estimate in (Rudjord et al. 2009) on the full-sky to $f_{NL} = 73 \pm 31$ using the KQ75 mask on the co-added V+W channel. We find no particular values of f_{NL} estimates close to the galactic plane and conclude that foregrounds are unlikely to affect the estimate of f_{NL} in the V and W bands even for the smaller KQ85 mask. In the Q band however, we find unexpectedly high values of f_{NL} in local estimates close to the galactic mask, as well as significant discrepancies between Q band estimates and V/W band estimates. We therefore conclude that the Q band is too contaminated to be used for non-Gaussianity studies even with the larger KQ75 mask. We further noted that the local f_{NL} estimates on the V+W channel are positive on all equatorial bands from the north to the south pole. The probability for this to happen in a universe with $f_{NL} = 0$ is less than one percent.

Subject headings: cosmic microwave background — cosmology: observations — methods: statistical

1. INTRODUCTION

Although the Cosmic Microwave Background (CMB) fluctuations are usually assumed to follow a Gaussian distribution, the consensus is that this is only an approximation valid to a certain level of precision. The deviations from Gaussianity seem to be small and are therefore difficult to estimate precisely. However, accurate knowledge of both the size and nature of such a deviation would be of high value in cosmology. The search for such anomalies in the CMB has therefore attracted much attention recently.

Most models for inflation predict the CMB fluctuation to be slightly non-Gaussian. This level of non-Gaussianity is measured by the parameter f_{NL} (see e.g. (Bartolo et al. 2004)). Alternative inflationary scenarios predict different values of f_{NL} , thus making an accurate estimate of this parameter crucial for understanding the physics of the inflationary era. Several f_{NL} parameters have been considered in the literature, corresponding to different ansatz for the shape of primordial non-Gaussianities. In this paper we focus on local non-Gaussianity, parametrized by f_{NL}^{local} (simply f_{NL} in the following).

In (Rudjord et al. 2009), we used needlets to estimate a value of $f_{NL} = 84 \pm 40$ (local type) different from zero at the 2σ level. This was in agree-

ment with previous estimates (Yadav & Wandelt 2008; Komatsu et al. 2009; Smith et al. 2009; Curto et al. 2008, 2009; Pietrobon et al. 2008, 2009) where values of f_{NL} deviating from zero with about 2σ were also reported. Also in agreement with previous estimates, we found that the value of f_{NL} increases with smaller sky cuts. This could be a result of smaller error bars due to the increased amount of data, or it could be an indication of foreground residuals near the galactic plane influencing the value of f_{NL} . This is our main motivation for estimating f_{NL} on smaller parts of the sky. By having local estimates of f_{NL} we can check whether the high value of f_{NL} comes from areas close to the galactic plane thus indicating the influence of foreground residuals, or whether consistent f_{NL} values are found in different parts of the sky. The second motivation for studying the directional dependence of f_{NL} , is due to several reports of the CMB deviating from statistical isotropy in various ways (Hansen et al. 2008; Groeneboom & Eriksen 2009; Hoftuft et al. 2009; Eriksen et al. 2004; Hansen et al. 2004; Vielva et al. 2004; Tegmark et al. 2003). Here we check whether a similar asymmetry is seen in the value of f_{NL} .

In (Rudjord et al. 2009), the bispectrum of spherical needlets (Lan & Marinucci 2008) was used to obtain f_{NL} . The localization and uncorrelation properties of needlets make them a convenient tool for studying localized regions on the sky (see (Baldi et al. 2006)). We will here use a similar analysis to estimate the level of non-Gaussianity on selected regions on the sky and in this way study the spatial variations of f_{NL} . We therefore refer the reader to (Rudjord et al. (2009)) for a more detailed description of the procedure, as well as for a more extensive list of references.

This paper is organized as follows. In section 2 we describe the data used for the analysis, in section 3 we describe the non-Gaussian maps and in section 4 we outline the method used for estimating f_{NL} . We apply the

¹ email: oystein.rudjord@astro.uio.no

² Institute of Theoretical Astrophysics, University of Oslo, P.O. Box 1029 Blindern, N-0315 Oslo, Norway

³ Centre of Mathematics for Applications, University of Oslo, P.O. Box 1053 Blindern, N-0316 Oslo, Norway

⁴ Dipartimento di Matematica, Università di Roma ‘Tor Vergata’, Via della Ricerca Scientifica 1, I-00133 Roma, Italy

⁵ Department of Applied Mathematics and Theoretical Physics, Centre for Mathematical Sciences, University of Cambridge, Wilberforce Road, Cambridge, CB3 0WA, United Kingdom

⁶ Dipartimento di Fisica, G. Galilei, Università di Padova and INFN, Sezione di Padova, via Marzolo 8, I-35131 Padova, Italy

procedure to *WMAP* data and present the results in section 5 before we summarize and conclude in section 6.

2. DATA

This analysis was performed using the foreground reduced co-added *V+W* frequency bands of the *WMAP* five year data at Healpix⁷ resolution $N_{side} = 512$. Also the individual Q, V and W bands were used for consistency tests. The Gaussian simulations were generated using the best fit power spectrum from the *WMAP* five year release. We also used the beam and noise properties supplied by the *WMAP* team. For masking out galactic foregrounds we used the *KQ75* as well as the smaller *KQ85* mask.

3. NON-GAUSSIAN MAPS

The non-Gaussian maps used for the analysis have been generated using the algorithm developed in (Liguori et al 2003; Liguori et al. 2007) (see also Elsner & Wandelt (2009) for recent developments). We briefly review the general structure of the algorithm here, while addressing the reader to the above mentioned papers for further details. The CMB multipoles $a_{\ell m}$ are related to the primordial gravitational potential Φ through the well known formula:

$$a_{\ell m} = \int \frac{d^3 k}{(2\pi)^3} \Phi(\mathbf{k}) Y_{\ell m}(\hat{k}) \Delta_{\ell}(k), \quad (1)$$

where $\Delta_{\ell}(k)$ is the radiation transfer function and the potential is written in Fourier space. However, for the case of primordial non-Gaussianity, the primordial potential takes a very simple expression in real space, where:

$$\Phi(\mathbf{x}) = \Phi_L(\mathbf{x}) + f_{\text{NL}} [\Phi_L^2(\mathbf{x}) - \langle \Phi_L^2(\mathbf{x}) \rangle]. \quad (2)$$

In the previous expression Φ_L is a Gaussian random field, characterized by a primordial power spectrum $P(k) = Ak^{n-4}$; in the following we will refer to $\Phi_L(\mathbf{x})$ as the Gaussian part of the primordial potential. The remaining non-Gaussian part of the potential is simply the square of the Gaussian part in each point (modulo a constant term, necessary to enforce the condition $\langle \Phi(\mathbf{x}) \rangle = 0$; however it is clear that this term affects only the CMB monopole)

It is then convenient to work directly in real space and recast formula (1) in the following form

$$a_{\ell m} = \int d^3 x \Phi(\mathbf{x}) Y_{\ell m}(\hat{x}) \Delta_{\ell}(r), \quad (3)$$

where $\Delta_{\ell}(r) \equiv \int dk k^2 j_{\ell}(kr) \Delta_{\ell}(k)$ are the real space transfer functions, $j_{\ell}(kr)$ is a spherical Bessel function, and r is a lookback conformal distance. This formula suggests to structure the algorithm in the following steps

1. Generate the Gaussian part Φ_L of the potential in a box whose side is the present cosmic horizon.
2. Square the Gaussian part point by point to get the non-Gaussian part.

⁷ <http://healpix.jpl.nasa.gov>

3. Expanding in spherical harmonics the Gaussian and non-Gaussian parts of the potential for different values of the radial coordinate r in the simulation box.
4. Convolve the spherical harmonic expansions of Φ_L and Φ_{NL} with the radiation transfer function $\Delta_{\ell}(r)$ in order to obtain the Gaussian and non-Gaussian part of the multipoles of the final NG CMB simulation. For a given choice of the non-Gaussian parameter f_{NL} a CMB map is then obtained simply through the linear combination $a_{\ell m} = a_{\ell m}^L + f_{\text{NL}} a_{\ell m}^{\text{NL}}$ (the superscripts L and NL always indicating Gaussian and non-Gaussian respectively).

The most difficult and time consuming part in this process is actually the generation of the Gaussian part of the potential Φ . The difficulty arise from the fact that we are working in a box of the size of the present cosmic horizon, that in conformal time is about 15 Gpc, but at the same time a cell in this box must have a size no bigger than 20 Mpc in order to resolve the last scattering surface, where most of the CMB signal is generated. It turns out (see Liguori et al (2003); Liguori et al. (2007) for details and more explanations) that a convenient way to achieve this is to work directly in spherical coordinates, use a non uniform discretization of the simulation box (since no points are needed in a large region of the box where photons are just free streaming) and generate the multipoles of the expansion of $\Phi_L(\mathbf{x})$ through the following two step approach:

1. Generate uncorrelated radial multipoles $n_{\ell m}(r)$, gaussianly distributed and characterized by the following spectrum:

$$\langle n_{\ell_1 m_1}(r_1) n_{\ell_2 m_2}^*(r_2) \rangle = \frac{\delta^D(r_1 - r_2)}{r^2} \delta_{\ell_1 \ell_2} \delta_{m_1 m_2}; \quad (4)$$

where δ^D is the Dirac delta function.

2. Filter the multipoles $n_{\ell m}$ with suitable functions in order to produce a Gaussian random field with the properties of the multipole expansion of the primordial Gaussian potential Φ_L . It can be shown that the expression of the filter functions is:

$$W_{\ell}(r, r_1) = \frac{2}{\pi} \int dk k^2 \sqrt{P_{\Phi}(k)} j_{\ell}(kr) j_{\ell}(kr_1), \quad (5)$$

where P_{Φ} is the primordial power spectrum, and the filtering operation takes the form

$$\Phi_{\ell m}^L(r) = \int dr_1 r_1^2 n_{\ell m}(r_1) W_{\ell}(r, r_1). \quad (6)$$

In the last expression $\Phi_{\ell m}^L(r)$ are the desired quantities i.e. the multipoles of the expansion of the Gaussian part of the primordial potential for a given r .

4. METHOD

The bispectrum has shown to be the most powerful tool for estimating f_{NL} . The bispectrum is zero for a Gaussian field, and any significant deviations from a zero bispectrum is therefore a non-Gaussian signal. Needlets are a new type of spherical wavelets which were introduced by (Narcowich et al. 2006). For our analysis we use the bispectrum of needlet coefficients (Lan & Marinucci 2008) to estimate f_{NL} . The localization properties of needlets make it possible to obtain the bispectrum in several different regions of the sky with very little additional costs in terms of CPU time compared to one full sky analysis. Although the needlet bispectrum does not yield optimal error bars on f_{NL} (see (Smith et al. 2009) for the optimal method), the advantage is the possibility of a fast and easy calculation of local estimates for consistency checks.

The needlet coefficients are denoted β_{jk}^B , j is frequency, k the direction on the sky (we will take k as the pixel number in the Healpix grid) and the parameter B characterizes the localization in frequency domain. Indeed, needlets allow for a tight control of localization in harmonic space and uncorrelation in pixel space; these properties are valuable for statistical inference and are not shared by other wavelet constructions, please refer to (Baldi et al. 2006), (Marinucci et al. 2008) for details and further references (see also (Pietrobon et al. 2006) and (Fay et al. 2008)). For instance, for a given value of B a needlet coefficient only contains information on multipoles in the range $\ell = [B^{j-1}, B^{j+1}]$. Thus, the parameter B controls localization in harmonic space: small values of B correspond to small ranges of frequencies j , while the reverse is true for larger B .

The needlet bispectrum with base B may be expressed as

$$I_{j_1 j_2 j_3}(\mathrm{d}\Omega) = \sum_k^{\text{pixels} \in \mathrm{d}\Omega} \frac{\beta_{j_1 k} \beta_{j_2 k} \beta_{j_3 k}}{\sigma_{j_1 k} \sigma_{j_2 k} \sigma_{j_3 k}} \quad (7)$$

where σ_{jk}^B are the standard deviation of the needlet coefficients β_{jk}^B for a Gaussian map and $\mathrm{d}\Omega$ is the region of the sky for which the bispectrum is calculated.

For the estimation of f_{NL} we used a similar procedure as in Rudjord et al. (2009), but with a few small changes. We used a higher value for B , resulting in fewer needlet scales. Intuitively one would expect this to give a poor result, since each needlet scale would cover a large interval in ℓ -space. However, a higher value for B also gives better localization properties in pixel-space, thus minimizing the influence of the mask and thereby reducing the error bars. Additionally, this greatly reduces the computational cost of the analysis.

We will calculate the needlet bispectra using the needlet coefficients calculated on the pixels k of a $N_{\text{side}} = 512$ map. We will use all the $N_{\text{side}} = 512$ pixels k which are inside an $N_{\text{side}} = 2$ pixel as our smallest region $\mathrm{d}\Omega$. We thus obtain 48 bispectra $I_{j_1 j_2 j_3}(p)$ where p denotes a pixel of the $N_{\text{side}} = 2$ pixelization. Having obtained these 48 bispectra it is straightforward to construct the bispectrum on sky patches with different shapes and sizes. We see from eq. 7 that the bispectrum of a larger patch is

then simply

$$I_{j_1 j_2 j_3}(\text{region}) = \sum_p I_{j_1 j_2 j_3}(p), \quad (8)$$

where the sum over p goes over the $N_{\text{side}} = 2$ pixels within the desired region.

In order to estimate f_{NL} we perform a χ^2 analysis for every map and region to be investigated

$$\chi^2(f_{NL}) = \mathbf{d}^T(f_{NL}) \mathbf{C}^{-1} \mathbf{d}(f_{NL}) \quad (9)$$

where the data vector is

$$\begin{aligned} \mathbf{d} &= I_{j_1 j_2 j_3}^{\text{obs}} - \langle I_{j_1 j_2 j_3}(f_{NL}) \rangle \\ &= I_{j_1 j_2 j_3}^{\text{obs}} - f_{NL} \langle \hat{I}_{j_1 j_2 j_3} \rangle. \end{aligned} \quad (10)$$

$\langle \hat{I}_{j_1 j_2 j_3} \rangle$ is here the average first order non-Gaussian bispectrum obtained using non-Gaussian simulations (Liguori et al. 2007). See (Rudjord et al. 2009) for details. The corresponding covariance matrix \mathbf{C} is evaluated by means of Monte-Carlo simulations.

Differentiating to find the value for f_{NL} which gives the lowest χ^2 yields the ‘‘Generalized Least Squares’’ estimate:

$$f_{NL} = \frac{\langle \hat{I}_{j_1 j_2 j_3} \rangle^T \mathbf{C}^{-1} I_{j_1 j_2 j_3}}{\langle \hat{I}_{j_1 j_2 j_3} \rangle^T \mathbf{C}^{-1} \langle \hat{I}_{j_1 j_2 j_3} \rangle}. \quad (11)$$

We estimate local f_{NL} values according to the procedure described in (Rudjord et al. 2009), but with one important difference: We calculate and save the bispectra calculated on each individual $N_{\text{side}} = 2$ pixel for each simulation. Then, when the bispectrum and thereby f_{NL} is estimated for a larger region, the bispectra for the different $N_{\text{side}} = 2$ pixels are added up according to eq. 8 and the correlation matrix is constructed from this final bispectrum for each larger region.

5. RESULTS

First we estimated f_{NL} on the full sky using $B = 1.781$ and 11 needlet scales covering multipoles up to $\ell_{\text{max}} = 1500$. This was the best trade-off (lowest error bars) between needlet coefficients for low values of B being more affected by the mask but having more frequencies j and for high values of B being less affected by the mask but having fewer scales. Otherwise we followed the same procedure as in Rudjord et al. (2009). The results are presented in table 1.

freq. channel	<i>KQ75</i>	<i>KQ85</i>
$V + W$	73 ± 31	78 ± 29
V	58 ± 35	55 ± 33
W	74 ± 37	72 ± 34
Q	-8 ± 39	-9 ± 37

TABLE 1
 f_{NL} ESTIMATES AND 1σ ERROR BARS. THESE ESTIMATES ARE FOUND USING THE FULL CMB SKY.

As we see from the results, the combined $V + W$ channel gives a 2σ deviation from Gaussianity. The individual V and W channels are consistent (within 2σ), but the Q

channel deviates significantly from the others, suggesting possible contamination by foregrounds.

We repeat the above analysis on localized regions on the sphere. First the bispectra were found for an ensemble of Gaussian simulations on each of the 48 ($N_{\text{side}} = 2$) Healpix patches on the sky. We then combined these patches in three different ways according to eq. 8.

1. **Hemispheres** The larger regions were defined to be hemispheres. For each of the 48 directions defined by the ($N_{\text{side}} = 2$) pixel centers, f_{NL} was estimated on a hemisphere centered on this direction.
2. **45° discs** Same as for the hemispheres, estimating f_{NL} on discs with 45° radius instead of hemispheres.
3. **Equatorial rings** These regions were defined to be the 7 constant latitude rings in which the $N_{\text{side}} = 2$ healpix pixels are ordered. Each of these rings covers a relatively small part of the sky, and the error-bars are therefore large. However they are not overlapping, and the f_{NL} estimates on the different rings can therefore be considered nearly independent (except for the largest scales).

The f_{NL} estimates from the 45° discs with the smaller *KQ85* mask are shown in figure 1, where each pixel represents the f_{NL} estimate on a disc centered on the pixel. The lower plot shows the same map, but f_{NL} for each region has been normalized by its standard deviation. We see that even for the smaller mask, there is no evidence for particularly high values of f_{NL} in the galactic region, but note that most of the values are positive. In figure 2 we show the corresponding map of f_{NL} estimates over hemispheres while using the *KQ75* mask. As an additional test of consistency we have produced the same estimates based on bispectra obtained from $N_{\text{side}} = 4$ pixels instead of $N_{\text{side}} = 2$ pixels. The result is shown in the same figure. We can see that the two maps show the same structures on the sky.

As seen from figure 1 the distribution of f_{NL} on the sky shows a dipole. For the f_{NL}/σ map of the 45° discs of the *V+W* channel (*KQ85*), the dipole has a maximum at $\theta = 129^\circ$, $\phi = 96^\circ$ with an amplitude of $T_{\ell=1}^{f_{NL}} = 61$. We investigated whether such a dipolar distribution of f_{NL} was common in Gaussian simulations and found the value of the dipole amplitude to be in good agreement with simulated maps. The dipole is therefore to be expected. Investigation of the hemisphere results as well as for the *KQ75* mask using both the combined *V+W* channel and the individual *Q*, *V* and *W* frequency channels yielded similar results.

In order to check whether the 48 estimates of f_{NL} were internally consistent, we combined the estimates to form a data vector $\mathbf{d} = [f_{NL}^1, f_{NL}^2, \dots, f_{NL}^{48}]$ for a χ^2 test. Simulations were then used to find a covariance matrix containing the covariances between the 48 estimates. Then a χ^2 test was performed on Gaussian simulations as well as on the *WMAP* data. The χ^2 values of the data were compared with those of the simulations. The results, both for the hemisphere estimates as well as for the 45° disk estimates, was that the χ^2 of the *WMAP* data was fully

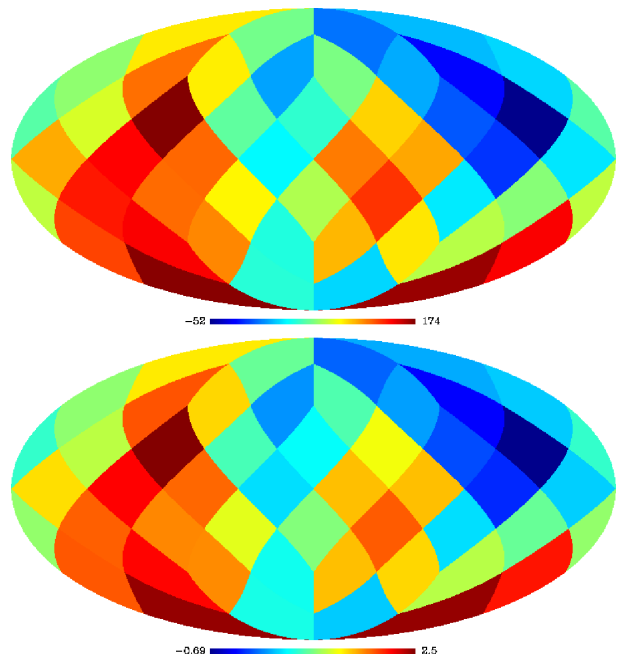


FIG. 1.— The upper figure shows f_{NL} estimates on 45° discs centered on the given pixels, while the lower figure shows the same estimates divided by their standard deviation. The estimates were made on the *V+W* channel using the *KQ85* galactic mask.

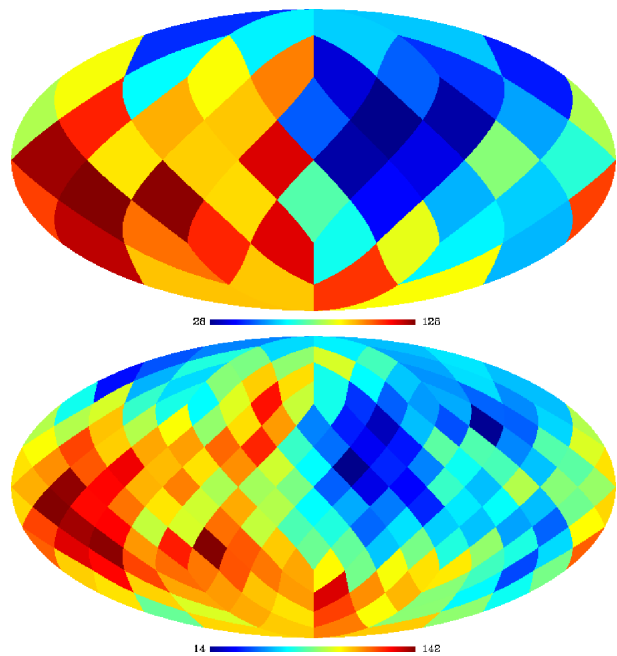


FIG. 2.— Both the figures shows f_{NL} estimates on hemispheres, but for the upper one the estimates are performed while using resolution $N_{\text{side}} = 2$, while for the lower one we have used $N_{\text{side}} = 4$. We can see that the two maps show the same structures. These estimates were made on the *V+W* channel using the *KQ75* galactic mask.

consistent with Gaussian simulations (within 2σ). The local f_{NL} estimates are therefore internally consistent.

As a further test we obtained estimates of f_{NL} on equatorial rings. The motivation behind this approach was to uncover possible foreground contamination outside the

KQ75 mask. The f_{NL} estimates for the different rings are presented in table 2. We see that the estimates of f_{NL} seem higher around equator, but the errors-bars are also larger (due to the galactic mask in the equatorial region). Since none of the rings show particularly high values (compared to the error bars) we do not have evidence to claim that foreground residuals have an influence of the estimates of f_{NL} . The internal consistency of the various ring estimates have been tested as described above and shown to be in agreement with simulations (within 2σ).

We also estimated f_{NL} on the equatorial rings of the $V + W$ map using the smaller *KQ85* mask. These results are presented in table 2. As expected the error-bars are somewhat smaller then the results with the *KQ75* mask, especially around the equatorial region. The estimates are consistent with the ones from the *KQ75* mask.

We then followed through with similar investigations of the individual Q , V and W frequency channels using the *KQ75* mask (table 2). The V and W channels are consistent (within 2σ), while only the Q channel shows a 3σ deviation in the ring around equator exactly where foreground residuals would be expected. We thus suspect a possible influence of foreground contamination in this band. This was further checked by testing the consistency of the estimated f_{NL} between the bands using a χ^2 approach. Whereas the (V - W) and (V - Q) differences were found to be consistent with simulations (within 2σ), the (W - Q) difference was found to be larger than in 99% of the simulations.

Also, a similar test was performed on the differences $f_{NL}(V) - f_{NL}(VW)$ and $f_{NL}(W) - f_{NL}(VW)$. We see in table 1 and on some rings in table 2 that the VW estimates seem driven by the W estimate. This is not seen in simulated maps and it was found that the small difference $f_{NL}(W) - f_{NL}(VW)$ found for the WMAP data is found in only 5% of the simulated maps whereas the difference $f_{NL}(V) - f_{NL}(VW)$ for WMAP was found to be consistent (well within 2σ) with simulations.

ring	$V+W$		Q	V	W
	<i>KQ75</i>	<i>KQ85</i>	<i>KQ75</i>	<i>KQ75</i>	<i>KQ75</i>
1	91 ± 95	93 ± 95	47 ± 118	66 ± 106	94 ± 111
2	11 ± 68	6 ± 68	-18 ± 83	1 ± 76	28 ± 79
3	80 ± 80	43 ± 71	-149 ± 100	19 ± 90	13 ± 93
4	283 ± 183	122 ± 113	700 ± 226	462 ± 205	253 ± 213
5	117 ± 82	128 ± 70	-61 ± 103	37 ± 92	122 ± 96
6	39 ± 66	53 ± 66	-81 ± 81	35 ± 74	15 ± 78
7	158 ± 93	156 ± 93	174 ± 114	138 ± 104	201 ± 108

TABLE 2

THE f_{NL} ESTIMATES AND 1σ ERROR-BARS FOR EQUATORIAL RINGS OF THE INDIVIDUAL Q , V , AND W FREQUENCY CHANNELS AS WELL AS THE CO-ADDED $V+W$ FOR THE MASKS *KQ75* AND *KQ85*.

We see that all of the rings for the $V+W$ channel (as well as the individual V and W channels) give a estimate $f_{NL} \geq 0$. These rings are nearly independent (except for the largest scales) and for a sky with $f_{NL} = 0$ one would expect that each of these have a 50% probability of being positive. For 7 rings one would then expect only a $\frac{1}{2^7} \approx 0.78\%$ probability that all rings give $f_{NL} \geq 0$ (this probability is confirmed by simulations).

Since the lowest value estimated for the rings of the $V + W$ channel (with the *KQ75* mask) is $f_{NL} = 11$, we investigated the probability of this occurring in Gaussian simulations. We found that of 4000 Gaussian simulations, only 0.35% have $f_{NL} \geq 11$ in all the rings.

6. CONCLUSIONS

In this paper we have used the bispectrum of needlets to obtain local estimates of f_{NL} on the WMAP five year data. We performed the analysis on the combined $V+W$ channel, as well as the individual Q , V and W channels, using multipoles up to $\ell = 1500$ and the *KQ75* galactic cut. For the combined $V+W$ channel we also applied the *KQ85* mask.

We first made a full sky analysis, resulting in a best fit value of $f_{NL} = 73 \pm 31$ for the combined $V+W$ channel using the *KQ75* mask. The individual V and W channels give consistent (within 2σ) results, but the f_{NL} estimate of the Q channel deviates significantly, suggesting contamination of foregrounds.

The estimates were then made on selected regions of the sky and showed how the needlet bispectrum approach is powerful for finding estimates of f_{NL} in many different regions, roughly at the cost of one single full sky estimate. We divided the sky into smaller regions according to four different patterns: hemispheres, 45° disks and equatorial rings. In each of these schemes f_{NL} was estimated in every region. The results were compared to simulations using a χ^2 test, and all local f_{NL} estimates were found to be internally consistent (within 2σ) for the V and W channels.

The local estimates of f_{NL} showed a dipolar distribution of f_{NL} on the sphere, with a maximum at $\theta = 129^\circ$, $\phi = 96^\circ$. For comparison, the hemispherical power asymmetry reported in Hansen et al. (2008) was found with a maximum in $\theta = 107^\circ$, $\phi = 226^\circ$, and is therefore not expected to be connected to the findings in this paper.

Also, such a dipolar distribution was found to be common in simulated Gaussian maps. For the equatorial rings we found a positive value for f_{NL} in every ring. We compared the lower estimate of the $V+W$ channel ($f_{NL} \geq 11$ for all rings) with simulations and found that only 0.35% of Gaussian simulations have this feature.

For the rings we find no significant evidence of foreground contamination outside the galactic *KQ75* mask. The results also seem to be fairly consistent (within 2σ) between the individual V and W channels whereas the Q band show signs of possible foreground contamination in the equatorial band where f_{NL} is larger than zero at the 3σ level. This is confirmed by the fact that the differences in local f_{NL} values between the Q and W bands are larger than in 99% of the simulations.

We conclude that our study shows no significant anisotropy in the estimates of f_{NL} in the CMB sky. No abnormal values for f_{NL} are found close to the equator except for the Q band where we suspect foregrounds to influence the estimate of f_{NL} .

FKH is grateful for an OYI grant from the Research Council of Norway. This research has been partially supported by ASI contract I/016/07/0 "COFIS" and ASI contract Planck LFI Activity of Phase E2. We acknowledge the use of the NOTUR supercomputing

facilities. We acknowledge the use of the HEALPix (Górski et al. 2005) package and the Legacy Archive for Microwave Background Data Analysis (LAMBDA).

Support for LAMBDA is provided by the NASA Office of Space Science.

REFERENCES

- Baldi, P., Kerkycharian, G., Marinucci, D. & Picard D. 2009, *Annals of Statistics*, Vol. 37, arXiv:math/0606599
- Bartolo, N., Komatsu, E., Matarrese, S. & Riotto, A. 2004, *Phys. Rept.*, 402, 103
- Curto, A. et al., 2008, arXiv:0807.0231
- Curto, A., Martinez-Gonzalez, E. & Barreiro, B. 2009, arXiv:0902.1523
- Elsner, F. & Wandelt, B. D., 2009, *ApJS* 184 264
- Eriksen, H. K., Hansen, F. K., Banday, A. J., Górski, K. M. & Lilje, P. B. 2004, *ApJ*, 605, 14
- Fay, G., Guilloux, F., Betoule, M., Cardoso, J.-F. Delabrouille, J., Le Jeune, M. 2008, *Phys.Rev. D*78:083013, arXiv:0807.1113
- Górski, K.M. et al. 2005, *ApJ*, 622, 759-771
- Groeneboom, N. E. & Eriksen, H. K. 2009, *ApJ*, 690, 1807
- Hansen, F. K., Banday, A. J. & Górski, K. M. 2004, *MNRAS*, 354, 641
- Hansen, F. K., Banday, A. J., Górski, K. M., Eriksen, H. K. & Lilje, P. B. 2008, arXiv:0812.3795
- Hoftuft, J. et al. 2009, in press, arXiv:0903.1229
- Komatsu, E. et al. 2009, *ApJS*, 180, 330
- Lan, X. & Marinucci, D., *Electronic Journal of Statistics* 2008, Vol. 2, 332-367, arXiv:0802.4020
- Liguori, M., Matarrese S. and Moscardini, L., 2003, *ApJ*, 597, 57
- Liguori, M. et al. 2007, *Phys. Rev. D*, 76, 105016
- Marinucci, D. et al. 2008, *MNRAS*, 383, 539
- Narcowich, F.J., Petrushev, P. & Ward, J.D. 2006, *SIAM Journal of Mathematical Analysis* 38, 2, 574
- Pietrobon, D., Balbi, A., Marinucci, D. 2006, *Physical Review D*, 74, 043524
- Pietrobon, D., Cabella, P., Balbi, A., de Gasperis, G. & Vittorio, N. 2008, arXiv:0812.2478
- Pietrobon, D. et al. 2009, arXiv:0905.3702
- Rudjord, O. et al 2009, arXiv:0901.3154
- Smith, K. M., Senatore, L. & Zaldarriaga, M. 2009, arXiv:0901.2572
- Tegmark, M., de Oliveira-Costa, A. & Hamilton, A. J. 2003, *Phys. Rev. D*, 68, 123523
- Vielva, P., Martinez-Gonzalez, E., Barreiro, R. B., Sanz, J. L. & Cayon, L. 2004b, *ApJ*, 609, 22
- Yadav, A. P. S. & Wandelt, B. D. 2008, *Physical Review Letters*, 100, 181301